Extended-range and faster photon-counting Brillouin optical time domain reflectometer

Maxime Romanet, Etienne Rochat, Jean-Charles Beugnot, Kien Phan Huy

OPTICA

Extended-range and faster photon-counting Brillouin optical time domain reflectometer

Maxime Romanet,[1] Étienne Rochat,[2] Jean-Charles Beugnot,[1,*] and Kien Phan Huy[1,3]

[1]FEMTO-ST Institute, Université de Franche-Comté, UMR CNRS 6174, 25030 Besançon, France
[2]Omnisens S.A., Morges, Switzerland
[3]SUPMICROTECH, Institut FEMTO-ST, 25000 Besançon, France
*jc.beugnot@femto-st.fr

Received 18 November 2024; revised 4 February 2025; accepted 4 February 2025; published 0 MONTH 0000

Distributed fiber optic sensors are used to monitor civil infrastructures and detect earthquakes and for energy transport surveillance. Over the past 20 years, various technological and numerical advances have pushed back the limits of these sensors and diversified their applications. However, the maximum range of distributed fiber optic sensors such as Brillouin optical time domain reflectometers (BOTDRs) is currently limited by the signal-to-noise level of the detectors. We present a fast, long-range measurement technique with a high signal-to-noise ratio that overcomes these difficulties. We propose to use a gated single-photon detector triggered by multiple gating pulses delayed by sub-dead time duration. The length of the pulse sequence considerably reduces measurement time without compromising spatial resolution, maximum range, or sensitivity. The proposed approach is demonstrated experimentally by measuring the Brillouin signal up to a distance of 150 km in a standard single-mode fiber. The measurements were performed without need for an optical amplification module remotely placed along a standard single-mode fiber, thus surpassing the state of the art and providing excellent agreement with theory. We experimentally demonstrate a hot-spot measurement at 125 km with a spatial resolution of 20 m. By extrapolating our results, we pave the way for the future 200 km BOTDRs.

https://doi.org/10.1364/OPTICA.549392

1. INTRODUCTION

Distributed optical sensors have rapidly developed over the last few decades, benefiting from enabling technologies such as laser and fiber optics [1,2]. They can measure temperature or strain at distances of tens or hundreds of kilometers, and are used to monitor pipelines and submarine cables, as well as earthquakes and geological activity [2–8]. Among these sensors, optical reflectometers send a pulse of light into the fiber under test. The light is then scattered backward by light-matter interaction, which can be Raman, Rayleigh, or Brillouin scattering. The backscattered light is then measured using an interferometric setup and a photodiode. Determination of the light's time of flight enables the location of the backscattering to be pinpointed, while temperature or deformation is determined from the properties of the backscattered light. Among these sensors, those based on Brillouin optical time domain reflectometry (BOTDR) have the particularity of producing an absolute temperature measurement. The use of conventional photodiodes allows a spatial resolution down to 10 cm [9,10] and a range of up to 100 km with a 10 m spatial resolution [11,12]. The current capabilities of BOTDR sensors allow for a range of up to 100 km using polarization-diverse coherent detection [12], and up to 250 km when combining Raman amplification with an erbium-doped amplifier [13,14]. The latter, along with other recent improvements, typically involves the integration of a new class of optical lasers within the fiber network or the introduction of specialty optical fiber.

Ultimately, the range of these sensors is limited by the signal-to-noise ratio (SNR) of the photodiode. This limitation can be overcome by quantum technologies such as single-photon avalanche photodiodes (SPADs) or superconducting nanowire single-photon detectors (SNSPDs) [15–18]. Sensors based on Rayleigh and Raman scattering [19–21] as well as Brillouin scattering [22,23] have been fabricated using these technologies. The latter sensor is called ν-BOTDR. However, the disadvantage of photon counting is the long measurement times involved. As a photon counter only counts one photon at a time, many measurements have to be taken to establish a statistic and calculate an optical power. In [22], the SPAD detector operates in *gated mode*, and a measurement cycle can be described as follows: once the pump light pulse is sent, an electrical pulse signal called a *gate* is sent to trigger the SPAD. This activation *gate* signal is delayed relative to the optical pulse by the time of flight required for the light to travel to the position of the measurement point and return to the detector. If the SPAD detector detects an incoming photon, a positive event is recorded. Thanks to the delay, backscattering is assumed to have occurred at the point of interest and the recorded event is associated with a position along the fiber. After detection,

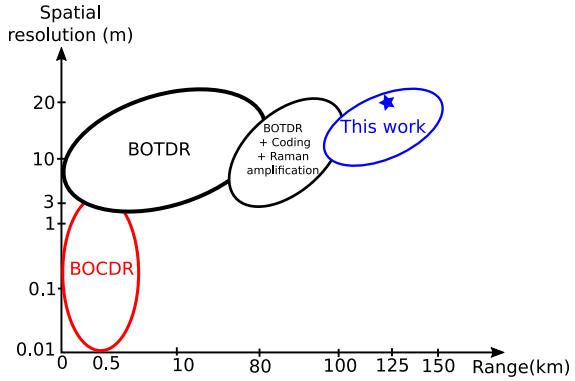

Fig. 1. Illustration of Brillouin optical reflectometry performance, provided for guidance only, in single-mode optical fiber at telecommunications wavelength without active optical amplification along optical fiber. Note that the experimental conditions may vary between articles. BOCDR: Brillouin optical correlation domain reflectometer [25,26], BOTDR [27,28], BOTDR assisted by Raman amplification [11,13], BOTDR assisted by coding and polarization diverse coherent detection [12], and ν-BOTDR [22].

the SPAD then becomes inactive for a necessary time, called dead time, to avoid false detections due to the after-pulsing effect [24]. After several experiment cycles, the proportion of positive events for a given time is used to determine the equivalent scattered optical power. This means that a measurement cycle detects only one position along the fiber. This leads to detrimental measurement times or poor resolution as shown by the total measurement duration:

$$T_{\text{total}} = \frac{x_{\max}}{\delta x} \times T_{\text{meas}}, \tag{1}$$

where $x_{\max}$ is the distance of the furthest measurement point (range), δx is the sampling interval, and T_{meas} is the required time to measure the temperature at one distance, which is here assumed to be constant. Better spatial resolution measurement increases the number of cycles and thus the total measurement duration. Conversely, traditional interferometric devices measure an entire length of fiber in a single cycle, as the light backscattered along the fiber is measured continuously by the photodiode.

In this article, we move closer to this mode of operation with a method we call *multi-gating*, which scans several points along the optical fiber in a single measurement cycle. This method, applied to the ν-BOTDR, enables us to measure Brillouin signal at a distance of 150 km while circumventing dead time limitations and maintaining good resolution. The SNR of our system allows us to achieve temperature measurements at a range of 125 km. Figure 1 compares our results with other BOTDR devices according to spatial resolution and range. The article is divided into three parts. First, we introduce our setup and the *multi-gating* approach. Then, experimental results are presented to show the ability to reach long-range temperature measurement and good resolution. Finally, we discuss measurement time and spatial resolution optimization for a given range.

2. EXPERIMENTAL SETUP

The experimental setup is represented in Fig. 2. A tunable narrowband laser sends infrared light into a semiconductor optical amplifier (SOA) surrounded by optical isolators to avoid the laser effect. The SOA generates optical pulses of duration T_{pulse} going from 10 to 200 ns, according to the chosen spatial resolution, with a measured peak power of 13.6 dBm.

A circulator C1 sends the optical pulses into the single-mode fiber under test (G.652.D) of 150 km with optical losses of 0.19 dB/km. The optical pulses generate Rayleigh and Brillouin scattered light in the backward direction that is collected through the circulator C1. A fiber Bragg grating (FBG) with a high rejection ratio of 40 dB is combined with a circulator C2 to filter the Rayleigh (red) and Brillouin Stokes (green) scattered light and measure only the Brillouin anti-Stokes (BAS) signal (blue) as illustrated by the spectrum inset in Fig. 2(a). Note that a similar approach was demonstrated by Wait and Hartog on conventional BOTDR [29]. Unlike [22], here we do not use the FBG as a frequency discriminator, but we position the BAS wavelength at the center of a flat FBG passband thanks to the tunability of the

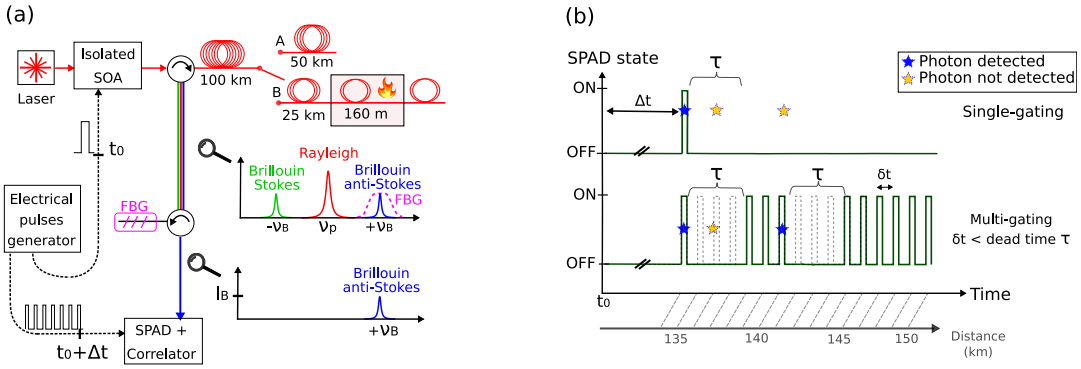

Fig. 2. (a) ν-BOTDR principle based on single-photon avalanche detector (SPAD), using a fiber Bragg grating (FBG) and *multi-gating* technique. t_0 corresponds to the trigger of the semiconductor optical amplifier (SOA), Δt is the delay between the trigger of the SOA and the activation of the SPAD. It corresponds to the round-trip photons' time of flight to the measurement position. Black dashed lines represent the microwave cables and solid lines the optical fibers. The spectrum (top) shows the backscattering spectrum from the optical fiber with the FBG response in a magenta dashed line. The second spectrum (bottom) shows the spectrum after filtering by the FBG, and corresponding to the Brillouin anti-Stokes signal (blue) measured on the SPAD. The Brillouin Stokes (green) and scattering (red) are attenuated by 40 dB thanks to the FBG. The Brillouin anti-Stokes light frequency is at the center of the FBG flat top bandpass, so that temperature fluctuation only affects the measured intensity. (b) Chronograms showing the different techniques with distributed measurements based on SPAD and the influence of dead time. Top: chronogram of the SPAD activation with a *single-gating* technique. The response along the optical fiber is done by modifying Δt to scan every point. Bottom: chronogram of the SPAD activation when the dead time, denoted τ, is larger than the intraburst delay δt. Multiple gates allow scanning different points along the optical fiber within the same cycle.

frequency of the laser. We would point out that it is also possible to carry out the measurement on the Brillouin Stokes signal, by shifting the laser frequency, to obtain the Stokes response at the center of the FBG. The power levels are equivalent between the Stokes and anti-Stokes signals. The temperature is extracted from the 0.38 %/K intensity dependence on the Brillouin anti-Stokes (BAS) intensity. This approach optimizes the signal-to-noise ratio with a better signal compared to the frequency discriminator approach. In order to measure weak signals from more than 100 km, we use a SPAD in gated mode (Geiger mode) [30] with a dark count rate per gate of 0.06 cps in our setup. To perform a measurement, after the light pulse is sent, an electrical pulse generator generates an activation gate pulse to trigger the SPAD for a short time:

$$T_{\text{gate}} = T_{\text{pulse}}/2. \tag{2}$$

Each activation gate corresponds to a particular distance along the optical fiber defined by the delay Δt between the optical pulse and the activation gate pulse. By choosing Δt as the time of flight taken for the light pulse to travel to the measurement point and back, we have a precise localization of the measurement position along the fiber. If a photon is detected by the SPAD, as shown by the blue star in the chronogram in Fig. 2(b), the time correlator receives an electrical pulse and assigns a *tag* to the corresponding gate. After a few hundred measurements, a statistic can be calculated, leading to the equivalent optical power

$$P = N_{\text{phot/s}} \frac{h\nu}{T_{\text{gate}} \times f}, \tag{3}$$

where $N_{\text{phot/s}}$ is the number of photons per second, h is the Planck constant, ν is the photon frequency, T_{gate} is the gate duration, and f is the cycle frequency. As shown in the chronogram at the top of Fig. 2(b), a detection (blue star) is followed by a dead time denoted τ, of typically 10 µs. During this period, no detection can be performed, in order to prevent false detections due to the after-pulsing effect [31,32]. Consequently, the sensor becomes *blind* for a period corresponding to a distance of about 1 km. If only one activation gate is opened per cycle, the dead time has no influence on the measurement, since the period of a cycle corresponds to 100 km. This is illustrated by the following yellow star in Fig. 2(b).

To minimize measurement time, we need to perform as many measurements as possible per cycle, and therefore open as many gates as possible in a pulse train without distorting the statistics due to dead time periods. In Fig. 2(b), we compare the SPAD activation chronogram for the two techniques, *single-gating* (top) and *multi-gating* (bottom). Each gate corresponds to a position along the optical fiber. In the *multi-gating* scheme [Fig. 2(b) bottom], some activation gate pulses are sent with a delay shorter than the dead time. This means we can scan more points along the optical fiber, but the statistic may be distorted by the deactivation of gates following a detection. In the chronogram, at the bottom of Fig. 2(b), the first photon detection (blue star) is followed by a missed photon (yellow star). This scenario would alter the statistics and give a poor estimate of power. However, in the low-flux regime, i.e., for distances greater than 100 km, this scenario is unlikely to occur. In this regime, the probability $p_{\text{detection}}$ of detecting a photon for any activation gate is well below one. The joint probability that two subsequent activation gates will result in two detections $p^2_{\text{detection}}$ is therefore even lower. Since the joint probabilities evolve according to a square law in the low-flux regime, many activation gates can be launched after a detection without altering the optical power estimate.

In general, the signal level after 100 km is less than 2 cps. A 100 ns gate has therefore a probability of 2×10^{-7} of producing a photon detection, making the joint probabilities of subsequent detections very low. Calculations and explanations of the distortion of the power as a function of distance are detailed in Supplement 1. In the following paragraph, we present experimental results obtained beyond 100 km to confirm this hypothesis.

3. EXPERIMENTAL RESULTS

In Fig. 3(b) the Brillouin anti-Stokes trace is plotted using 200 ns optical pulses, with 500 activation gates (in black) thanks to the multi-gating method. The complete trace was obtained in 1 h. In Fig. 3(a), the complete measurement of the optical fiber is shown, by measuring different parts of the optical fiber and adjusting the attenuation with a variable attenuator, in order to avoid saturation of the SPAD and high-flux regime (see Supplement 1). At the connection between the two different coils (at 100 km), the signal drops due to a poor connection, and a difference of Germanium doping. The total length of the optical fiber is 150.5 km and the signal measured over this distance corresponds to the noise level of our sensor. The noise is mainly due to the amplified spontaneous

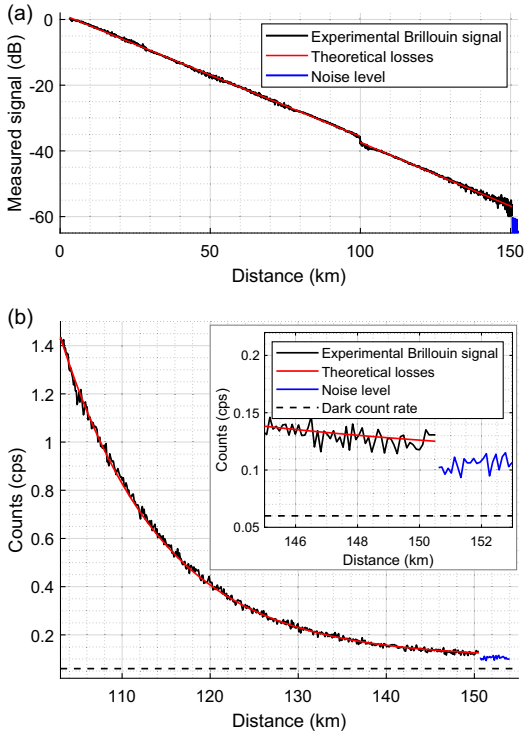

Fig. 3. Distributed measurement of the Brillouin anti-Stokes signal with 200 ns optical pulses (a) on the different optical fiber spools. One of 100 km (0.187 dB/km) measured with a variable attenuator, and the one of 50 km (0.194 dB/km) without attenuator. Measurement realized with 1.8 million of averaging. (b) Measurement of the last part of the optical fiber, with a cumulated acquisition time of 1 h. The dark count rate (DCR) is shown by the dashed black line (DCR = 0.06 cps). Inset shows a zoom on the end of the trace, where the signal after 150.5 km is out of the fiber. The vertical axis represents the count rate (cps). 500 gates are opened per cycle time $T = 1.6$ ms, with an intraburst delay $\delta t = 1$ µs, so that any detection would be followed by 10 gates within the dead time (10 µs).

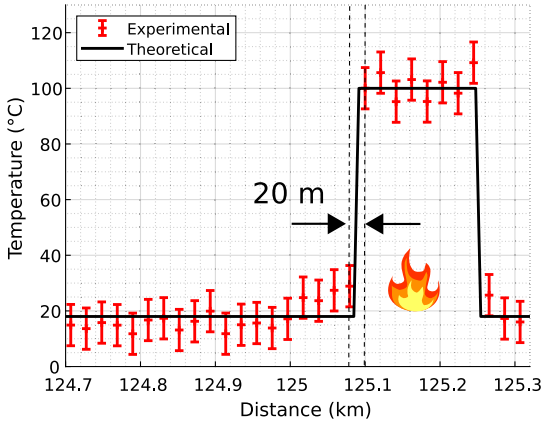

Fig. 4. Temperature profile made with the setup B in Fig. 2(a). We show the area around 125 km with a spatial resolution of 20 m. The 150 m heated fiber is in an oven heated to 100°C. The ambient temperature is 19°C and the acquisition time is set to 3 h. Experiment realized with a dead time $\tau = 10$ µs and an intraburst delay $\delta t = 200$ ns.

emission (ASE) from the SOA and the dark count rate (DCR) of the SPAD. The inset in Fig. 3(b) allows us to observe the difference between the Brillouin signal, the ASE, and the DCR. At 150.5 km the level of signal-to-noise ratio is around 1 dB. The theoretical curve in red solely based on the fiber attenuation, measured with a commercial optical time domain reflectometer (OTDR), shows a very good agreement. It confirms that the statistics are not distorted by the dead time while decreasing the total measurement time by a factor of 500.

In the following, we discuss temperature measurement and spatial resolution. Brillouin backscattering gain in optical fiber depends on temperature and strain as demonstrated in [28,33]. In our configuration, we use the dependence of the Brillouin anti-Stokes amplitude as a function of the temperature. The single-mode fiber (G.652D) used has been characterized in an adjustable oven and as a temperature coefficient of 0.38%/K. Optical fiber losses of the different sections of the fibers were first measured with a commercial OTDR, based on Rayleigh scattering. Using a reference OTDR trace, with an accuracy better than 0.01 dB (σ), we can compensate for optical losses when measuring the Brillouin anti-Stokes signal along the fiber. This compensation allows for a relative temperature measurement unaffected by optical losses, leveraging the temperature coefficient for accuracy. As we are measuring intensity variation, the stability of the laser power is crucial. However, laser power fluctuations can be monitored in real-time and compensated for when computing the detected photon flux. The chosen temperature reference is 19°C, corresponding to the ambient temperature in the laboratory.

We place 150 m of optical fiber inside an oven heated to 100°C, after 125 km of optical fiber. We get the temperature profile shown in Fig. 4(b). This measurement confirms the hypothesis of a low-flux regime, because the measured temperature is in good agreement with the heated oven temperature. Moreover, the measurement confirms the spatial resolution of 20 m as the 150 m of heated fiber are identified.

In Table 1 the standard deviation of the temperature measurement around 125 km is calculated for 21 different positions as a function of the acquisition time. After 1 h of measurement, the standard deviation drops below 9°C, and 4°C after 3 h of acquisition. This shows that one can spend more time on a certain area of interest to obtain more sensitive temperature measurements on that area. The *multi-gating* method therefore makes it possible to measure further quickly and without distortion, while maintaining good resolution and sensitivity.

Table 1. Standard Deviation of Temperature Measurements around 125 km, Averaged on 21 Close Positions, at Room Temperature

Acquisition time (h)	1	2	3
Standard deviation σ (°C)	8.5	5.7	3.7

4. MEASUREMENT TIME AND SPATIAL RESOLUTION

The expected advantage of the *multi-gating* method is the reduction of the acquisition time T_{total} compared to previous work [22]. T_{total} can be assessed with Eq. (1), taking for the single measurement the duration

$$T_{\text{meas}} = \frac{N_{\text{necessary counts}}}{N_{\text{phot/s}}(x_{\text{max}}) \times \eta_{\text{SPAD}}}, \tag{4}$$

where $N_{\text{necessary counts}}$ is the number of actual detections required to compute the statistics. Here 700 detections are necessary, corresponding to the measurement of 1 h represented in Table 1, where the standard deviation σ is below 9°C. x_{max} is the maximum distance of measurement, and η_{SPAD} is the SPAD efficiency (typically 20%). Note that for each point, T_{meas} is assumed to be constant and estimated with the Brillouin photon flux $N_{\text{phot/s}}(x_{\text{max}})$ at maximum distance, where it is the lowest. In Fig. 5, we show the calculation of T_{total} as a function of the number of gates and of the range for a 10 m sampling interval and a 20 m spatial resolution. The range corresponds to measurements made from 100 km to a distance x_{max} going up to 150 km.

One can see on the bottom right of the figure that measurements up to 150 km, with a 20 m resolution, require more than one month with *single-gating* operation as shown by the orange-yellow color in this area. As the number of gates is increased, the colors turn to green or blue, showing a significant decrease in total measurement time. Four white lines have been added to show 10 min, 30 min, 1 h, and 3 h measurements. On the top right of the figure, the lines show that the 150 km range can be fully measured within 6 h when 5000 activation gates per cycle are used. Moreover, the

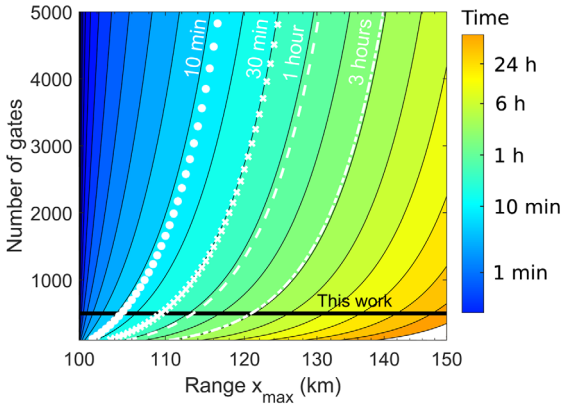

Fig. 5. Simulation of the acquisition time to detect 700 Brillouin photons in ν-BOTDR configuration. The sampling interval is 10 m and the spatial resolution is 20 m. The fiber section under test ranges from 100 km to distance x_{max}.

1 h dotted-dashed line shows that 130 km range falls into 30 min total measurement time. A significant improvement is therefore obtained. As long as the number of gates does not add distortion to the statistics, the number of gates is limited by the duration of the dead time, and also the flux of Brillouin photons. Supplement 1 gives details on this limitation.

As much as the challenge is to keep the total acquisition time low, we must achieve it while maintaining an acceptable spatial resolution for submarine applications. For BOTDR [34], spatial resolution is defined by

$$\Delta x = \frac{c \times T_{\text{pulse}}}{2n}, \tag{5}$$

where T_{pulse} is the optical pulse duration, c the speed of light in vacuum, and n the effective group index of the optical fiber. The optical pulse duration affects the Brillouin efficiency [34] but also the activation gate duration because they are linked by Eq. (2). Both phenomena alter the signal-to-noise ratio (SNR), the former because it modifies the BAS signal, and the latter because it affects the noise. Indeed, the duration upon which the SPAD detector is activated has an impact on the measurement noise that results from the optical noise of the experimental setup and the dark count rate, which is a property of the SPAD detector. As a consequence, one must also consider the SNR when investigating the spatial resolution. The SNR writes

$$\text{SNR} = 10 \times \log_{10}\left(\frac{\eta_{\text{SPAD}} \times N_{\text{phot/s}} + N_{\text{noise}}}{N_{\text{noise}}}\right), \tag{6}$$

where the noise detection rate's N_{noise} main contributions are the dark count rate and the amplified spontaneous emission (ASE) coming from the SOA and coupled through the circulator with an isolation of 62 dB. To calculate the SNR, we made measurement of the Brillouin efficiency with optical pulses ranging from 10 to 200 ns and measured dark count rates for the corresponding activation gates. Using Eqs. (3), (5), and (6) we then calculated the spatial resolution for the maximum achievable range providing a minimum SNR of 1 dB. The result is shown in red in Fig. 6. By increasing the spatial resolution, the detection range can be extended while maintaining the SNR at 1 dB, because more photons are injected into the optical fiber with longer T_{pulse}. The figure shows how a ν-BOTDR can be configured to favor the maximum range over spatial resolution or the other way around.

The maximum performance of ν-BOTDR has not yet been reached. One of the limitations of our setup is that the power injected is limited to 13.6 dBm, which corresponds to the maximum output power achievable with an extinction ratio of 68.2 dB. Indeed, the ν-BOTDR technique needs a high extinction ratio to prevent the continuous background noise between each optical pulse from degrading the photon counter readings as it passes through the circulator (C1). To improve the performance of our ν-BOTDR, a higher peak power for optical pulses is desirable. However, distributed sensors based on Brillouin scattering are limited by maximum peak power and background noise to avoid modulation instability and pump depletion. In particular, it is commonly accepted that 200 mW is the limit to avoid a nonlinear detrimental effect [35,36] and that ASE filtering is required.

The second limitation is due to the detection system. The SPAD efficiency in this study is 20%, with a DCR of 0.06 cps. For commercial SPADs, improving efficiency will degrade the DCR and, consequently, the SNR of the detection system. Thanks to the development of quantum technologies, new operating regimes have been explored to increase the activation frequency of SPADs [37,38], and detectors with a reduced after-pulsing probability [39] and also superconducting nanowire single-photon detectors (SNSPDs) have emerged. SNSPDSs offer greater efficiency, up to 80% with a DCR estimated at less than 0.01 cps [40]. This new technology offers the possibility to improve the SNR by 20 dB, thanks to a lower DCR and a higher efficiency.

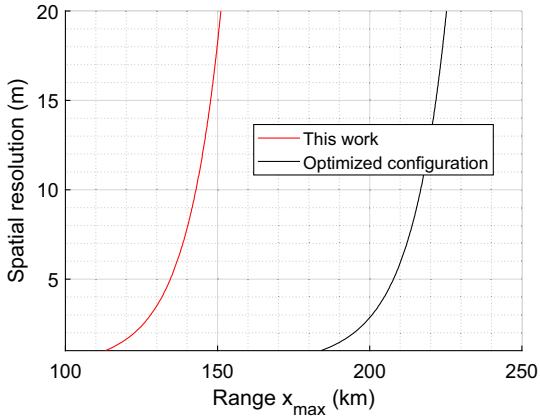

Fig. 6. Comparison between the actual configuration (red) and the simulated ν-BOTDR response (black) with commercial SNSPD with an efficiency of 80% and optical pump pulse power of 23 dBm (ASE filtering).

Combining the increased power of optical pulses with the state of the art of single-photon detection counters, we find as shown in black in Fig. 6 that ν-BOTDR would achieve total ranges in excess of 200 km with sub-10 m resolution.

5. CONCLUSIONS

We have demonstrated a Brillouin optical reflectometer with long range, high signal-to-noise ratio, and short measurement time. Using multiple gates per cycle to trigger the SPAD detector considerably reduces acquisition time. We have confirmed this *multi-gating* approach experimentally by demonstrating a hot-spot measurement at 125 km with a spatial resolution of 20 m and an acquisition time of less than 3 h. These measurements are in good agreement with theory, which shows no distortion despite the fact that SPADs are used in gated mode with a sub-dead time pulse delay. This is due to the low probability of subsequent detections at distances greater than 100 km. As a result, a significant reduction in measurement time is achieved while maintaining good performance in terms of range, spatial resolution, and SNR. We also showed that the saving in measurement time can be devoted to improving temperature sensitivity. In addition, we have demonstrated a ν-BOTDR measurement over a distance of 150 km and a temperature measurement at 125 km without optical amplification along a standard single-mode fiber, surpassing the state of the art.

Finally, we are paving the way for the ν-BOTDR to exceed 200 km by optimizing the pump power while maintaining an excellent extinction ratio, and improving the efficiency of the detector [41]. The *multi-gating* could be applied to all photon-counting technology measurements involving low-flux signals, such as medical imaging or spectroscopy.

Funding. European Interreg VI program; Ministère de l'Enseignement supérieur, de la Recherche et de l'Innovation; Conseil régional de Bourgogne-Franche-Comté; Agence Nationale de la Recherche (ANR-17-EURE-0002).

Acknowledgment. We thank Jean-Marc Merolla for fruitful discussions and technological support.

Disclosures. The authors declare no conflicts of interest.

Data availability. Data underlying the results presented in this paper are not publicly available at this time, but may be obtained from the authors upon reasonable request.

Supplemental document. See Supplement 1 for supporting information of the methodology used.

REFERENCES

1. A. Motil, A. Bergman, and M. Tur, "State of the art of Brillouin fiber-optic distributed sensing," Opt. Laser Technol. **78**, 81–103 (2016).
2. A. H. Hartog, *An Introduction to Distributed Optical Fibre Sensors* (CRC Press, 2017).
3. H. H. Kee, G. P. Lees, and T. P. Newson, "All-fiber system for simultaneous interrogation of distributed strain and temperature sensing by spontaneous Brillouin scattering," Opt. Lett. **25**, 695–697 (2000).
4. J. Li, W. Zhu, E. Biondi, *et al.*, "Earthquake focal mechanisms with distributed acoustic sensing," Nat. Commun. **14**, 4181 (2023).
5. B.-J. Wang, K. Li, B. Shi, *et al.*, "Test on application of distributed fiber optic sensing technique into soil slope monitoring," Landslides **6**, 61–68 (2009).
6. Y. Yin, H. Wang, Y. Gao, *et al.*, "Real-time monitoring and early warning of landslides at relocated Wushan Town, the Three Gorges Reservoir, China," Landslides **7**, 339–349 (2010).
7. L. Zeni, L. Picarelli, B. Avolio, *et al.*, "Brillouin optical time-domain analysis for geotechnical monitoring," J. Rock Mech. Geotech. Eng. **7**, 458–462 (2015).
8. N. J. Lindsey, T. C. Dawe, and J. B. Ajo-Franklin, "Illuminating seafloor faults and ocean dynamics with dark fiber distributed acoustic sensing," Science **366**, 1103–1107 (2019).
9. Y. Koyamada, Y. Sakairi, N. Takeuchi, *et al.*, "Novel technique to improve spatial resolution in Brillouin optical time-domain reflectometry," IEEE Photonics Technol. Lett. **19**, 1910–1912 (2007).
10. Y. Mizuno, N. Hayashi, H. Fukuda, *et al.*, "Ultrahigh-speed distributed Brillouin reflectometry," Light Sci. Appl. **5**, e16184 (2016).
11. M. Song, Q. Xia, K. Feng, *et al.*, "100 km Brillouin optical time-domain reflectometer based on unidirectionally pumped Raman amplification," Opt. Quantum Electron. **48**, 30 (2015).
12. T. Jostmeier, B. Marx, C. Buntebarth, *et al.*, "Long-distance BOTDR interrogator with polarization-diverse coherent detection and power evaluation," in *Optical Fiber Sensors* (2020), paper T3-21.
13. P. Clement, R. Gabet, V. Lanticq, *et al.*, "Enhancement of sensing range of Brillouin optical time-domain reflectometry system up to 150 km with in-line bi-directional erbium-doped fibre amplifications," Electron. Lett. **57**, 142–144 (2021).
14. T. Joy, T. Jostmeier, B. Marx, *et al.*, "Increasing the distance range of repeaterless Brillouin-otdr to 250 km by optical amplification," in *Optical Fiber Sensors* (2022), paper W1-3.
15. Z.-P. Li, J.-T. Ye, X. Huang, *et al.*, "Single-photon imaging over 200 km," Optica **8**, 344–349 (2021).
16. L. A. Jakob, W. M. Deacon, O. Hicks, *et al.*, "Single photon multiclock lock-in detection by picosecond timestamping," Optica **8**, 1646–1653 (2021).
17. F. Madonini, A. A. Maurina, and F. Villa, "Spad sensors for time-gated Raman spectroscopy," in *Microscopy Histopathology and Analytics* (2022).
18. S. Ly, G. McNerney, S. Fore, *et al.*, "Time-gated single photon counting enables separation of cars microscopy data from multiphoton-excited tissue autofluorescence," Opt. Express **15**, 16839–16851 (2007).
19. B. Li, G. Deng, R. Zhang, *et al.*, "High dynamic range externally time-gated photon counting optical time-domain reflectometry," J. Lightwave Technol. **37**, 5899–5906 (2019).
20. M. Höbel, J. Ricka, M. Wüthrich, *et al.*, "High-resolution distributed temperature sensing with the multiphoton-timing technique," Appl. Opt. **34**, 2955–2967 (1995).
21. C. Antony, J. Hayes, and P. D. Townsend, "Single-photon detector based long-range fibre-optic distributed temperature sensor," in *Optical Instrumentation for Energy and Environmental Applications* (2012), paper ET4D-5.
22. M. Romanet, L. M. Giraldo, M. Zerbib, *et al.*, "Towards single-photon Brillouin optical time domain reflectometry," Opt. Express **31**, 21542–21552 (2023).
23. L. Xia, J. Hu, Q. Zhao, *et al.*, "A distributed Brillouin temperature sensor using a single-photon detector," IEEE Sens. J. **16**, 2180–2185 (2016).
24. A. D. Mora, D. Contini, A. Pifferi, *et al.*, "Afterpulse-like noise limits dynamic range in time-gated applications of thin-junction silicon single-photon avalanche diode," Appl. Phys. Lett. **100**, 241111 (2012).
25. H. Lee, K. Noda, Y. Mizuno, *et al.*, "Distributed temperature sensing based on slope-assisted Brillouin optical correlation-domain reflectometry with over 10 km measurement range," Electron. Lett. **55**, 276–278 (2019).
26. Y. Mizuno, Z. He, and K. Hotate, "One-end-access high-speed distributed strain measurement with 13-mm spatial resolution based on Brillouin optical correlation-domain reflectometry," IEEE Photonics Technol. Lett. **21**, 474–476 (2009).
27. T. Kurashima, T. Horiguchi, H. Izumita, *et al.*, "Brillouin optical-fiber time domain reflectometry," IEICE Trans. Commun. **76**, 382–390 (1993).
28. S. M. Maughan, H. H. Kee, and T. P. Newson, "Simultaneous distributed fibre temperature and strain sensor using microwave coherent detection of spontaneous Brillouin backscatter," Meas. Sci. Technol. **12**, 834–842 (2001).
29. P. Wait and A. Hartog, "Spontaneous Brillouin-based distributed temperature sensor utilizing a fiber Bragg grating notch filter for the separation of the Brillouin signal," IEEE Photonics Technol. Lett. **13**, 508–510 (2001).
30. P. Eraerds, M. Legré, J. Zhang, *et al.*, "Photon counting OTDR: advantages and limitations," J. Lightwave Technol. **28**, 952–964 (2010).
31. A. Gallivanoni, I. Rech, and M. Ghioni, "Progress in quenching circuits for single photon avalanche diodes," IEEE Trans. Nucl. Sci. **57**, 3815–3826 (2010).
32. S. Cova, M. Ghioni, A. Lacaita, *et al.*, "Avalanche photodiodes and quenching circuits for single-photon detection," Appl. Opt. **35**, 1956–1976 (1996).
33. M. Niklès, L. Thévenaz, and P. A. Robert, "Brillouin gain spectrum characterization in single-mode optical fibers," J. Lightwave Technol. **15**, 1842–1851 (1997).
34. T. Horiguchi, K. Shimizu, T. Kurashima, *et al.*, "Development of a distributed sensing technique using Brillouin scattering," J. Lightwave Technol. **13**, 1296–1302 (1995).
35. M. N. Alahbabi, Y. T. Cho, T. P. Newson, *et al.*, "Influence of modulation instability on distributed optical fiber sensors based on spontaneous Brillouin scattering," J. Opt. Soc. Am. B **21**, 1156–1160 (2004).
36. M. Alem, M. A. Soto, and L. Thévenaz, "Analytical model and experimental verification of the critical power for modulation instability in optical fibers," Opt. Express **23**, 29514–29532 (2015).
37. A. Restelli, J. C. Bienfang, and A. L. Migdall, "Single-photon detection efficiency up to 50% at 1310 nm with an InGaAs/InP avalanche diode gated at 1.25 GHz," Appl. Phys. Lett. **102**, 141104 (2013).
38. J.-M. Merolla, D. Le Gac, L. Jacquinot, *et al.*, "A new GHz high-speed near-infrared uncooled single photon detector," in *International Conference on Space Optics (ICSO)* (2024), p. 058.
39. Z. Lu, W. Sun, Q. Zhou, *et al.*, "Improved sinusoidal gating with balanced InGaAs/InP single photon avalanche diodes," Opt. Express **21**, 16716–16721 (2013).
40. I. Esmaeil Zadeh, J. Chang, J. W. Los, *et al.*, "Superconducting nanowire single-photon detectors: A perspective on evolution, state-of-the-art, future developments, and applications," Appl. Phys. Lett. **118**, 190502 (2021).
41. S. Farina, I. Labanca, G. Acconcia, *et al.*, "10-nanosecond dead time and low afterpulsing with a free-running reach-through single-photon avalanche diode," Rev. Sci. Instrum. **93**, 053102 (2022).